

Al-Cu alloy formation by aluminium underpotential deposition from $\text{AlCl}_3 + \text{NaCl}$ melts on copper substrate

B. S. Radović¹, V. S. Cvetković², R. A. H. Edwards¹, J. N. Jovičević^{2*}

¹ *Institute for Advanced Materials, Joint Research Centre, I 21020 Ispra, Italy*

² *Faculty of Sciences and Mathematics, University of Priština, 38220 K. Mitrovica, Serbia*

Received 7 October 2009, received in revised form 10 December 2009, accepted 10 December 2009

Abstract

Aluminium was incorporated into copper electrode surface by underpotential deposition from equimolar $\text{AlCl}_3 + \text{NaCl}$ melt at 200 °C, 250 °C and 300 °C. The process was studied by linear sweep voltammetry and potentiostatic deposition/galvanostatic stripping. The deposits were characterized by electron probe (EMPA), glancing incidence X-ray diffraction (GIXRD) and Auger electron spectroscopy (AES). The electrochemical measurements showed clear evidence of formation of four intermetallic compounds. This was confirmed by the physical analysis, which showed four layers of successive bulk intermetallic compounds. However, the diffraction patterns of copper samples after two hours of aluminium underpotential deposition at 200 °C and 250 °C showed the diffraction peaks that we could not attribute to any in the literature cited Al/Cu intermetallic compound. The 2θ values (degrees) for unattributable diffraction peaks are reported. The constant-potential regions measured during the low-current stripping corresponded to the coexistence of pairs of the four intermetallic phases. The kinetics of growth of the identified compounds is described.

Key words: aluminium-copper alloys, underpotential deposition, diffusion, microscopy and microanalysis techniques, Gibbs energy of formation, kinetics

1. Introduction

Electrodeposition of metals and alloys is essential for a variety of industries including electronics, optics, sensors, automotive and aerospace, to name but a few. It has been extensively elaborated in [1–4].

However, neither aluminium nor its alloys can be electrodeposited from aqueous solutions because hydrogen is evolved before aluminium is plated. Aluminium and its alloys are important materials for the fabrication of corrosion resistant, lightweight, high-strength structures. Small additions of aluminium can also significantly improve properties of other metals [5]. The desire to electrodeposit metals and their alloys such as Al, Ti and W was the main driving force for non-aqueous electrolytes.

Among the non-aqueous solvents that have been used successfully to electrodeposit metals and their alloys [6–9], as well as aluminium and its metal alloys [10, 11], are the chloroaluminate molten salts [12,

13], which contain inorganic [12–17] or organic [12, 18–21] chloride salts combined with anhydrous aluminium chloride. The chloroaluminate molten salts seem to be ideal solvents for the electrodeposition of metal-aluminium alloys because they constitute a reservoir of reducible aluminium-containing species, they are excellent solvents for many metal ions, and they exhibit good intrinsic ionic conductivity [12, 13, 19–22].

The deposition of metals on foreign metal substrate at electrode potentials more positive than the Nernst-potential of the corresponding three-dimensional deposited metal bulk phase (UPD) [23, 24] has been a subject of research for more than fifty years [23–30]. The phenomenon of UPD from melts [12, 20, 31, 32] was documented in the case of aluminium UPD from inorganic [12, 14, 33–35] and organic melts (ionic liquids) [7, 12, 36–38].

Work on UPD of metals from solutions revealed that a metal, electrodeposited onto a metal cathode into which it could diffuse at room temperature, could

*Corresponding author: tel.: ++381 063 343140; fax: ++381 28 425398; e-mail address: matori47@hotmail.com

make a surface alloy with the substrate [39–44]. This was also realised for aluminium UPD from inorganic [12, 14, 33, 39–48] and organic melts [12, 38, 49, 50].

Electrodeposited alloys may differ considerably in their chemical and phase constitution from alloys of the same chemical composition but obtained by metallurgical (thermal) methods. The problem was examined in the past [1, 2], and more recently [12], showing some important cases of UPD alloys with phase structure differing from that of metallurgical alloys.

UPD of metals from solutions [25–29] and formation of alloys by UPD of aluminium from inorganic melts onto surface of different metals [14, 33–35] has been a subject of our work for more than twenty years. Initially, we observed aluminium UPD from $\text{AlCl}_3 + \text{NaCl}$ melt on several metal electrodes [14] inducing surface alloy formation. Our more elaborate study of aluminium UPD on Au [33, 34] and Ag [33, 35] revealed formation of four Au-Al and two Ag-Al alloys formed by diffusion of underpotentially deposited aluminium into gold and silver substrate, respectively. Similar results were obtained by others on gold [38, 51] and copper [7, 12, 36, 38] from organic melts. The differences observed most probably result from the difference in the deposition temperatures. Working temperatures in organic chloroaluminate melts range between 20 °C and 100 °C, while in inorganic melts working temperatures start well above these. It has been shown that temperature influences thermodynamics and kinetics of UPD of metals [26]. Higher temperatures promote reaction between the substrate and the depositing element, and solid-state interdiffusion dependence on temperature is also well known. The differences in anions present in the electrolytes used are of some importance, too [27, 28, 52, 53].

There are records of aluminium overpotential deposition [12, 26 and 31] and UPD [14, 26, 38, and 50] on copper substrate and Cu-Al alloy formation from organic melts – ionic liquids. However, there are no detailed studies of aluminium UPD on copper from inorganic chloroaluminate melts in the literature.

In the present study, the UPD of aluminium on polycrystalline substrate of copper from $\text{AlCl}_3 + \text{NaCl}$ equimolar melts was investigated by electrochemical techniques and surface analysis. The data on the influence of temperature and deposition time were correlated with the analysis results to produce data describing the thermodynamics and kinetics of the formation of several intermetallic compounds.

2. Experimental details

2.1. Electrochemical experiments

All electrochemical experiments were carried out in an electrochemical cell designed for work with melts,

under a purified argon atmosphere [13, 22, 35]. The cell was made of Pyrex glass and placed in a furnace.

Aluminium wire 3 mm in diameter (99.999 % pure, Alfa Products, Thiokol/Ventron division, USA) was used as a reference electrode in a Luggin capillary whose tip was placed close to the working electrode. This was to minimize the error in the measured potential associated to IR drop in the melt between the tip of the Luggin capillary and the working electrode. An aluminium plate (99.999 % pure, Alfa Products, Thiokol/Ventron division, USA) was used as a counter electrode. Two types of sizes of working electrode were used. The one for electrochemical experiments consisted of 1 mm diameter 99.99 % pure copper wire pressed into a glass tube of slightly larger diameter such that only 1 cm² area of the metal wire was exposed to the melt. The other was 2 cm² 99.99 % pure copper plate working electrode for surface/sub-surface analysis. It was clipped (above the melt surface) onto a conductive wire pressed into a glass tube.

The aluminium reference and counter electrodes were first mechanically polished consecutively on emery papers of grade 0, 00, 000, and 0000, and then on polishing cloths (“Beuhler Ltd.”) impregnated with alumina (“Banner Scientific Ltd.”) of 1 μm, 0.3 μm and 0.05 μm grades. After undergoing mechanical polishing procedure, the aluminium reference and counter electrodes were subsequently etched in solutions of 50 vol.% HF + 15 vol.% H₂O and conc. NH₄OH + 5 vol.% H₂O₂ prior to each experiment. All glassware was washed with triple distilled water and alcohol and dried at 120 °C for at least one hour before use.

The working electrodes for electrochemical experiments were mechanically polished and before introduction into the process each metal working electrode was chemically polished [25, 54]. The polishing mixture for copper electrode was 33 vol.% HNO₃ + 33 vol.% glacial acetic acid + 33 vol.% orthophosphoric acid. The electrode was immersed into the acid mixture heated to 60 °C and stirred for 10–15 s and then rinsed with plenty of tap water and eventually with triply distilled water.

The working electrodes-samples for surface/sub-surface analysis were mechanically polished with emery papers. Initially the largest grade was used and then progressively smaller ones down to the 0000 emery paper, until the electrode had a mirror-like appearance free from scratches or blemishes. All mechanical polishing steps were always performed manually rather than on a polishing machine, which was less convenient to use. The electrode was then chemically polished as described above.

Examination of the electrode surface under the optical microscope and with X-ray emission spectroscopy revealed no contaminating elements.

Sodium chloride (NaCl p.a., “Merck”) and aluminium (III) chloride (99.99 % pure AlCl_3 , “Aldrich

Chemical Company, Inc.”) were used for melt preparation.

Since aluminium (III) chloride is extremely sensitive to moisture and oxygen, special attention was paid to the chemicals and to the melt preparation. The sodium chloride was reduced to fine powder, dried in a furnace at 500 °C for five hours and kept in vacuum at 120 °C until use, in order to remove bonded water. This procedure was counter-productive for drying aluminium (III) chloride that absorbed water irreversibly during any handling. Therefore no drying procedure was applied; instead, fresh, sealed bottle of anhydrous AlCl₃ was used for each experiment. The procedure of melting the AlCl₃ + NaCl mixture consisted of heating (in inert atmosphere) a vessel with AlCl₃, at the bottom and NaCl on top at 250 °C, where upon all the AlCl₃ sublimed forming a homogeneous AlCl₃ + NaCl melt by reaction with NaCl. The melt was subjected to pre-electrolysis between two aluminium (99.999 % pure) plates with large surface area (20 cm² each) at 220–250 °C with constant current density $i = 1.5 \times 10^{-2} \text{ A cm}^{-2}$ for 10 h. Both aluminium plates were cleaned before use, in the same way as the reference electrode. After the pre-electrolysis, linear sweep voltammogram performed on vitreous carbon cathode in the melt showed only double layer charging and discharging features in the potential region between 0.005–1.85 V vs. Al.

Two different electrochemical techniques were used in the experiments: linear sweep voltammetry (LSV) and potentiostatic UPD followed by galvanostatic stripping. Two different procedures of LSV were carried out one after the other, as follows:

a) The potential range was scanned from a potential 0.050–0.100 V negative to the open circuit potential of the copper electrode (0.8–0.850 V measured against the aluminium reference electrode) to a potential 0.010–0.150 V positive to the reversible aluminium potential, followed by the return scan. The sweep rate was 0.010 V s⁻¹;

b) Then the same potential range was scanned except that the scan was interrupted when the potential reached 0.010–0.150 V positive to the reversible aluminium potential, and this potential was held for $\tau_d = 1, 3, 6, 9,$ and 15 min before starting the return scan. The sweep rate was as in a).

The procedure for the potentiostatic UPD followed by galvanostatic stripping was as follows:

a) The specimen was held at 0.050–0.100 V negative to the open circuit potential of copper (0.8–0.850 V vs. Al), to strip any aluminium already deposited. Then the potential was stepped to the 0.010–0.150 V from the reversible potential of aluminium;

b) This potential ($E_d = 0.010\text{--}0.150 \text{ V vs. Al}$) was maintained for $\tau_d = 1, 3, 6, 9, 15$ min, after which the potential was switched out of circuit to open the electrode circuit. The electrode potential was then re-

corded by an XY recorder as a function of time, whilst a small current ($\cong 0.02 \text{ mA cm}^{-2}$) slowly stripped the aluminium from the surface copper specimen. If the stripping current was interrupted for a few seconds, the measured potential did not detectably change. This shows that the activation overpotential caused by the stripping current was negligible and the potentials measured can be considered open circuit potentials.

All electrochemical measurements were carried out using a Universal programmer (PAR-M175), a potentiostat (PAR-M173) and an X-Y-t recorder (Hewlett Packard M7040A). The temperature of the melt was monitored by a chromel-alumel thermocouple with an accuracy of 1 °C.

2.2. Surface/sub-surface analysis

Glancing incidence X-ray diffraction (GIXRD) and electron microprobe analysis (EMPA) of polished cross-sections were used as techniques for surface/sub-surface analysis. These techniques were applied comparatively to blank probes polished mechanically and chemically and to samples after electrochemical UPD. Sample preparation for the surface/sub-surface analysis was as follows: aluminium was electrodeposited from the equimolar AlCl₃ + NaCl melt at constant underpotential ($E_d = 0.010\text{--}0.150 \text{ V vs. Al}$) for different periods of time ($\tau_d = 1, 2$ and 4 h) at three different temperatures ($t = 200 \text{ °C}, 250 \text{ °C}$ and 300 °C). Deposition was started 5 min after insertion of the working electrode in order to allow thermal equilibrium. The working electrode was then removed from the melt whilst still under polarization, then washed repeatedly under distilled water, air dried and stored in a desiccator until use.

The crystallographic structure present near the surface of these specimens was determined using glancing angle X-ray diffraction at an incident angle of 1° to the surface. A multipurpose glancing angle X-ray spectrometer using a standard X-ray tube and germanium solid-state detector was used. An IBM-PC-XT computer controlled the spectrometer with Superior electric microstepping motors powering various goniometric motions. The detector pulses were timed and counted using a Tecmar Lambaster interface.

To prepare cross-sections for EMPA examination, samples that had been used as working electrodes were first cut into smaller plates, typically 1/3 of the original size. These were supported vertically in clips and covered with conductive plastic powder. The sample in powder was then pressed into a disc (2.5 cm diameter and 1 cm height) and the remaining visible edge of the sample polished to 0.1 mm. EMPA was carried out using a CAMEBAX-R electron microprobe.

AES was used to obtain the composition-depth profile of the specimen under the surface.

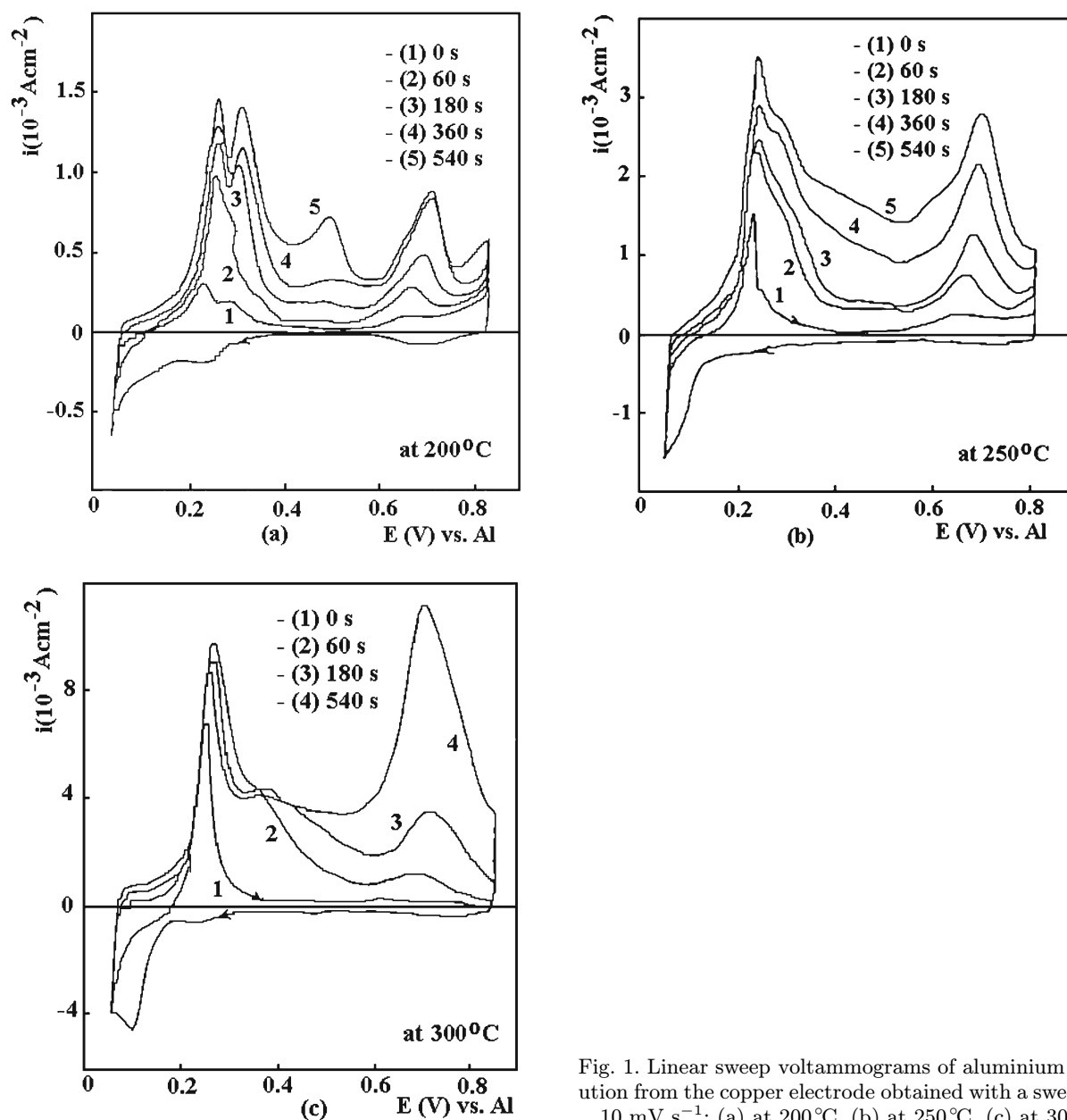


Fig. 1. Linear sweep voltammograms of aluminium dissolution from the copper electrode obtained with a sweep rate 10 mV s^{-1} : (a) at 200°C , (b) at 250°C , (c) at 300°C .

3. Results

Examples of the linear sweep voltammograms for aluminium underpotential deposition on copper electrodes at different deposition times (τ_d) and at various temperatures (t) are shown in Fig. 1. The potential values E (V vs. Al) and the corresponding current densities i ($10^{-3} \text{ A cm}^{-2}$) for the dissolution peaks observed in the anodic parts of the voltammograms, as a function of the deposition time τ_d and temperature t , are summarized in Table 1. The total anodic dissolution charge $Q_{\text{Al,max}}$ and calculated mass of aluminium deposited on copper electrodes, as a function of the deposition time and temperature, are listed in Table 2. $Q_{\text{Al,max}}$ values were obtained

by integration of the linear sweep voltammograms to give the surface area bounded by the anodic current and the horizontal axis. The values E , i_p and $Q_{\text{Al,max}}$ presented in Tables 1 and 2 are average values obtained from five or more measurements. The mass of aluminium deposited was calculated from Faraday's law.

Representatives of the potential/time diagrams of aluminium dissolution from copper electrodes, obtained by low-current galvanostatic stripping ("open circuit measurements") following UPD of various times and different temperatures, are given in Fig. 2. Table 3 summarizes the average potential values at the observed plateaux for five or more measurements.

An example of the diffraction patterns taken of the

Table 1. Peak potentials E (V vs. Al) and the corresponding anodic current densities i (10^{-3} A cm^{-2}) observed in the anodic part of linear sweep voltammograms on copper electrodes as a function of deposition time τ_d (s) and temperature t ($^{\circ}\text{C}$)

τ_d (s)	0		60		180		360		540	
t ($^{\circ}\text{C}$)	E	i								
200	0.22	0.31	0.26	0.99	0.25	1.18	0.25	1.28	0.26	1.47
	0.29	0.02	–	–	0.3	1.02	0.3	1.12	0.3	1.3
	–	–	0.47	0.07	0.49	0.16	0.52	0.32	0.51	0.72
	0.67	0.09	0.68	0.26	0.7	0.47	0.72	0.84	0.72	0.9
250	0.25	1.62	0.25	2.32	0.25	2.42	0.25	2.89	0.25	3.51
	0.66	0.25	0.68	1.76	0.68	1.38	0.72	2.18	0.72	2.78
300	0.24	6.89	0.25	8.82	0.25	9.01	0.25	9.41	0.25	9.88
	–	–	0.36	4.16	0.39	4.32	–	–	–	–
	–	–	0.73	1.02	0.71	3.62	0.71	7.23	0.7	11.42

Table 2. Total anodic dissolution charges (mC cm^{-2}) and mass calculated of Al deposited (10^{-6} g cm^{-2}) as a function of deposition time τ_d (s) and temperature t ($^{\circ}\text{C}$) for copper electrodes

t ($^{\circ}\text{C}$)	τ_d (s)	0	60	180	360	540
200	Total anodic charge	6.2	17.3	22.8	33.3	38.7
	Mass of Al deposited	0.58	1.63	2.14	3.13	3.64
250	Total anodic charge	13.41	40.2	58.8	87.5	122
	Mass of Al deposited	1.26	3.78	5.53	8.23	11.47
300	Total anodic charge	37.4	122.8	165.8	216.9	268.8
	Mass of Al deposited	3.51	11.5	15.58	20.39	25.27

Table 3. Inflection points and the corresponding values E (V vs. Al) obtained in “open circuit“ measurements of aluminium deposited on copper at different times τ_d (s) and various temperatures t ($^{\circ}\text{C}$)

t ($^{\circ}\text{C}$)	200			300		
τ_d (s)	60	180	540	180	360	540
Inflection point potential	0.19	0.16	0.16	0.24	0.22	0.22
	0.32	0.29	0.3	0.31	0.29	0.28
	–	0.49	0.49	–	–	–
	–	0.70	0.68	0.65	0.63	0.63

copper samples after aluminium underpotential deposition as a function of temperature and deposition time is given in Figs. 3, 4. The phases and their crystallographic systems identified in the deposits obtained are listed in Table 4. The phases were identified using JCPDS files [55–57] and the reference for each phase is also supplied.

The diffraction patterns of copper samples obtained after two hours of aluminium deposition at 250°C showed the diffraction peaks (denoted by symbol ?), which we could not attribute to either copper [55], aluminium [56] or any in the literature cited Al/Cu intermetallic compound. In the same time

X-ray fluorescence analysis showed no impurities present.

The 2θ values (degrees) for unattributable diffraction peaks are summarized in Table 5.

EMPA maps of aluminium distribution at the edge of copper samples after two hours of aluminium underpotential deposition at 250°C are shown in Fig. 5. The copper sample was analysed at 20 kV. A copper-aluminium layer is formed at the surface, but it is not very uniform, and has cracked away from the surface in places. The oxygen map (Fig. 5d) confirms that the layer is Cu-Al intermetallic compound, and not an oxide.

Table 4. The phases identified on copper samples after aluminium deposition at different times and various temperatures together with their crystallographic systems and references

t (°C)	τ_d (h)	Identified phase	System	Reference
200	2	(unidentified phase)	–	–
250	1	Al ₄ Cu ₉	cubic	[57]
	2	(unidentified phase)	–	–
	4	Al ₄ Cu ₉	cubic	[57]
300	2	Al ₄ Cu ₉	cubic	[57]

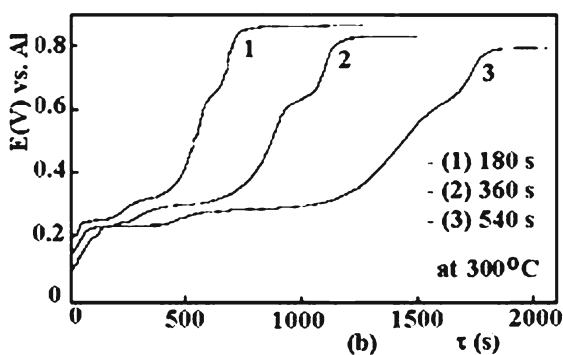
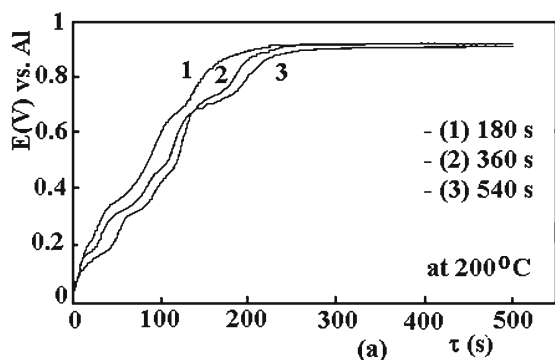


Fig. 2. “Open circuit” graphs of aluminium dissolution after UPD of aluminium on copper electrode: (a) at 200°C, (b) at 300°C.

Examples of the Auger depth profiles of aluminium into copper, as a function of temperature and deposition time, are given in Fig. 6 and summarized in Table 6.

4. Discussion

4.1. Linear sweep voltammograms: influence of deposition time and temperature

The reversible potential of copper was more positive than the reversible potential of aluminium in the

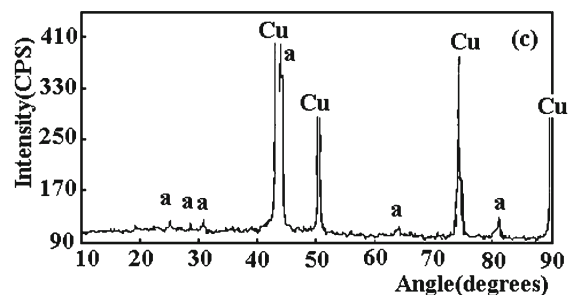
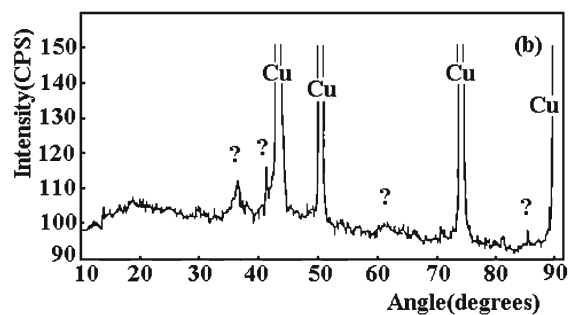
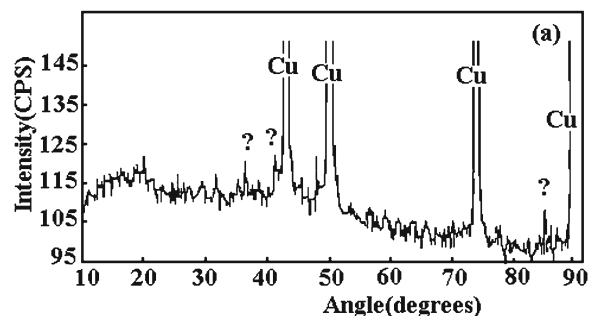


Fig. 3. Diffraction patterns of the copper samples after two hours of aluminium underpotential deposition: (a) at 200°C, (b) at 250°C, (c) at 300°C.

same system. This allowed a wide potential range, anodic to the aluminium reversible potential, i.e. the aluminium underpotential deposition region, to be studied.

In general, the fine structure of the cathodic current peaks of linear sweep voltammograms was less

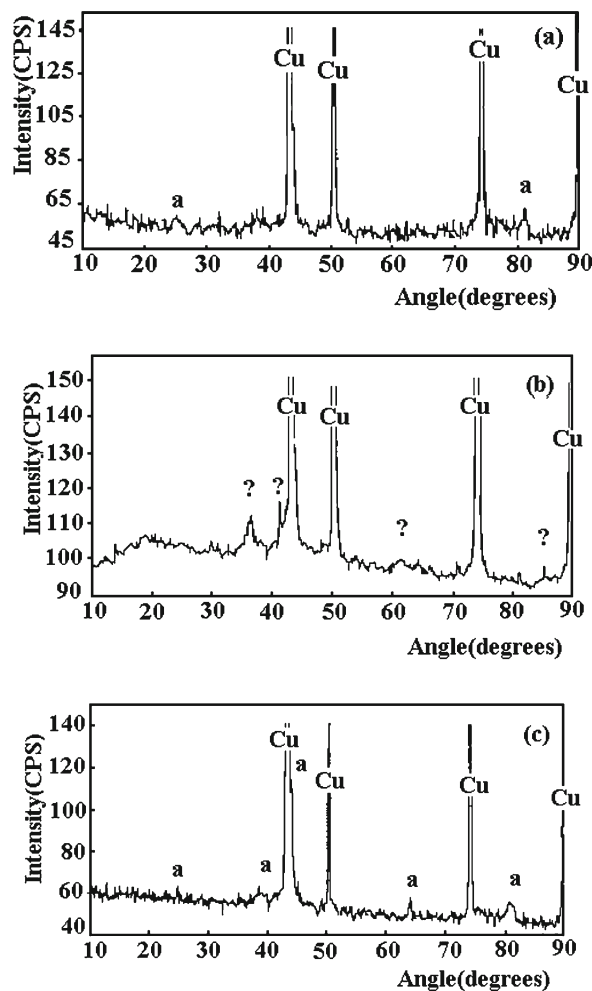


Fig. 4. Diffraction patterns of copper samples after: (a) one hour, (b) two hours, (c) four hours of aluminium underpotential deposition at 250°C.

Table 5. 2θ values (degrees) for unattributable X-ray diffraction peaks from the diffraction patterns of copper samples after two hours of aluminium underpotential deposition at 200°C and 250°C

t (°C)	τ_d (h)	2θ
200	2	36.6°, 41.4°, 85.1°
250		36.6°, 41.4°, 61.6°, 5.1°

pronounced than the anodic one. The anodic current peaks were more readily defined, particularly in the case of a prolonged underpotential deposition.

Ideally, one should record the potential at the beginning of corresponding anodic and cathodic peaks. Instead, in this case the current peak potential values were measured between peak valleys values. This was done for two reasons:

- cathodic peak separation was not as well pronounced as in the case of single crystal substrates [36,

Table 6. The depths (μm) of the formed aluminium layers on copper samples after aluminium underpotential deposition at different times and different temperatures and the technique used to establish given depths

t (°C)	τ_d (h)	Depth (μm)	Technique
200	2	0.3	AES
250	1	up to 1 μm	EMPA
	2	up to 1 μm	EMPA
	4	up to 1 μm	EMPA
300	2	0.6	AES

38–43, 49, 50], which prevented exact cathodic to anodic peak attribution;

- anodic current peaks were well merged thus preventing exact allocation of the peak starting potential.

In general, the total recorded charges bounded by the cathodic and anodic currents were similar (within $\pm 5\%$ difference) and symmetrical to the zero current axes.

The charges calculated for cathodic and anodic parts of the linear sweep voltammograms obtained, were significantly different from the charge needed for the deposition of the closest packed aluminium monolayer (Al atomic radius being 1.18×10^{-10} m) we calculated to be 1.17 mC cm^{-2} .

When the chosen cathodic end potentials, E_d , were maintained for longer times during linear sweep experiments, the cathodic current increase was not observed. This would suggest that the aluminium underpotential deposition after at least one aluminium monolayer completion proceeds at the rate necessary to compensate for the amount lacking of one aluminium monolayer, which entered solid state intermetallic reaction with the substrate – copper. This dynamic quasi-equilibrium would seem to be maintained as long as intermetallic solid-state reaction proceeded by diffusion of aluminium into the substrate. Different anodic dissolution peaks would then reflect different intermetallic compounds formed during previous aluminium deposition, having naturally different dissolution potentials [7, 34, 35] (Fig. 1).

When the holding (the deposition time, τ_d) of the copper electrode at the cathodic end potential, E_d , was increased, two characteristics of the anodic current peaks could be observed:

- anodic peak current values, i_p , increased with the cathodic end potential holding time τ_d ;

- the integrated charge under each of the anodic peaks (as well as the total anodic charge, $Q_{\text{Al,max}}$) increased proportionally to the square root of the cathodic end potential holding time $\tau_d^{1/2}$ (see Tables 1, 2 and Fig. 7).

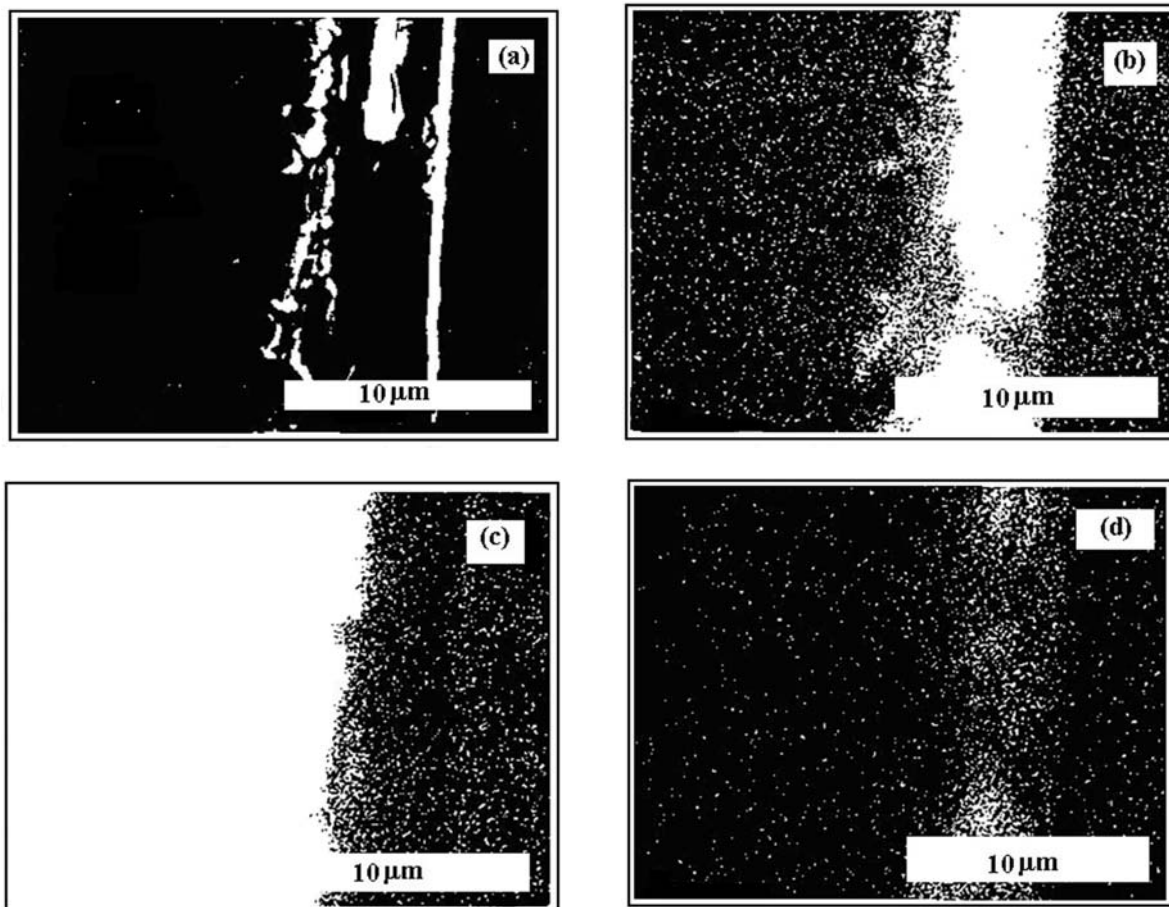


Fig. 5. EMPA maps of elemental distribution at the edge of copper sample: (a) secondary electron image, (b) Al $K\alpha$ emission map, (c) Cu $K\alpha$ emission map, (d) O $K\alpha$ emission map (marker 10 μm).

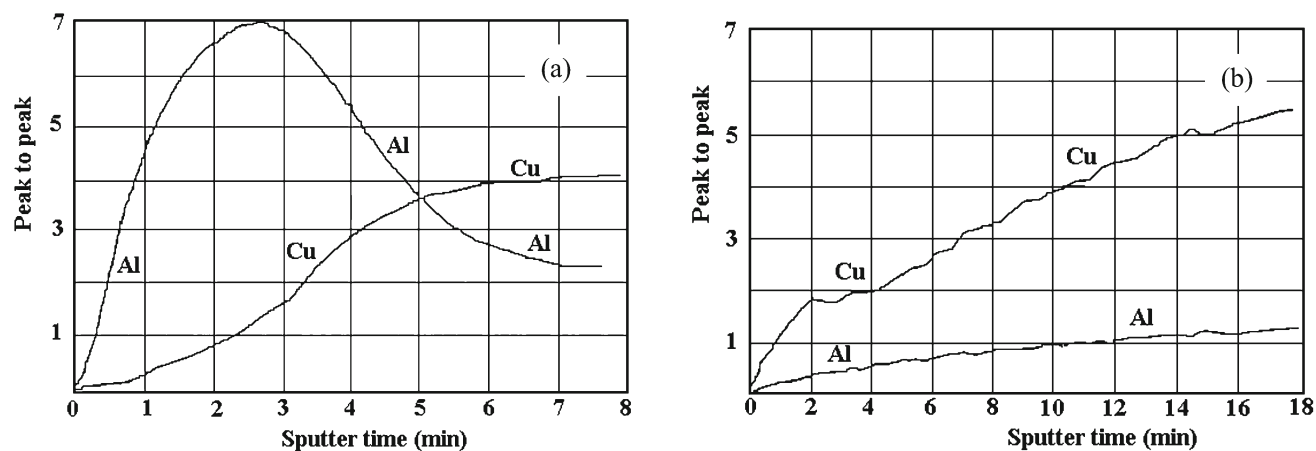


Fig. 6. Auger depth profiles of copper samples obtained after two hours of aluminium underpotential deposition: (a) at 200°C with sputtering rate 415 $\text{\AA} \text{min}^{-1}$, (b) at 300°C with sputtering rate 330 $\text{\AA} \text{min}^{-1}$.

It should be noted that the increase in working temperature of the system, all other conditions being kept the same, led to an increase of the charge under both cathodic and anodic peaks. Also, as it can be seen in Table 1, the anodic peak current values increased

with increasing working temperature.

LSV data obtained strongly suggest that, under the given conditions, underpotentially deposited aluminium diffuses into copper substrate forming surface alloys [34, 35].

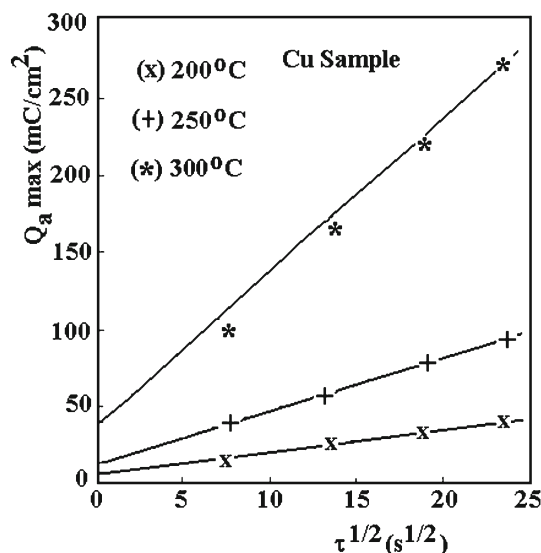


Fig. 7. Charge of aluminium dissolution $Q_{Al(\max)}$, as a function of $\tau^{1/2}$, at 200°C, 250°C and 300°C for copper electrode.

4.2. Low-current galvanostatic stripping

To obtain the dissolution characteristics of the underpotentially deposited aluminium onto and into the copper substrate, the potential pulse with amplitude cathodically exceeding the potentials characteristic for the appearance of anodic peaks ($E_d = 0.01\text{--}0.15$ V vs. Al) was followed by a quasi-open circuit measurement of the electrode potential with time. The small constant dissolution current applied in the “open circuit” measurements resulted in the potential-time curves exhibiting plateaux brought about by dissolution material being able to sustain an equilibrium potential (or corrosion potential) with $AlCl_4^-$ in the melt, Fig. 2. The number of plateaux (Table 3) can be seen to agree with the number of anodic peaks obtained during the linear sweep measurements (Table 1). The potentials of the four plateaux in Fig. 2 correspond reasonably well to the potentials of the anodic current peaks in the LSV’s. The existence of peaks in the linear sweep voltammograms indicates that these potentials are indeed reversible potentials (irreversible potential contributions such as activation overpotentials or diffusion overpotentials would increase monotonically with overpotential, and not result in peaks).

In fact, when the cathodic pulse amplitude applied was more negative than the potential of the most anodic peak observed on the linear sweep voltammogram, the plateau at the potential similar to the linear sweep voltammogram peak potential was recorded in the potential-time of curve of the “open circuit” measurement. When potential pulse amplitude exceeded both linear sweep voltammogram peak poten-

tials, the potential-time curves of the “open circuit” showed four plateaux at the potentials very close to the voltammogram peak potentials. This allowed the charge belonging to each of the plateaux (aluminium-copper intermetallic compounds) produced during potential step to be calculated on the basis of the time it took to be dissolved (dissolution current density being constant at 0.02 mA cm⁻²). The charges of cathodic deposition processes corresponded well with the anodic dissolution charges (within $\pm 3\%$) calculated as the multiple of dissolution current density and the time elapsed for the dissolution. Comparison of the charges obtained in this way agreed very well (within $\pm 5\%$) with the charges under the anodic peaks limited by the same potential range in the LSV voltammetry.

Prolonged potentiostatic underpotential deposition brought about a proportional increase in the “open circuit” dissolution time, but this had little effect on the potentials of the plateaux. An increase in the working temperature, however, increased the amount of aluminium deposited and dissolved. This is again consistent with the previously described linear sweep voltammetry results [34, 35].

The “open circuit” measurements, and particularly:

- the existence of the reversible (or corrosion) potential (four of them apart from reversible potential of copper substrate),
- the temperature dependence of these potentials,
- very similar behaviour of these potentials and the reversible aluminium potential,

gave strong support to the assumptions already made earlier that intermetallic compounds were formed between copper substrate and underpotentially deposited aluminium.

4.3. Alloy formation

Both the linear sweep voltammograms of aluminium deposition/dissolution (Fig. 1) and low-current galvanostatic stripping measurements (Fig. 2) clearly show that some interaction between the substrate and aluminium from the melt occurs at a potential positive to the potential of the aluminium reference electrode. If there were a nucleation barrier for alloy formation, one would expect an increase in the cathodic current during holding at the cathodic-end potential. No such increase was observed, indicating dynamic quasi-equilibrium was maintained at the surface by diffusion of the aluminium into the metal substrate. Since it is known that copper [58, 59] makes several intermetallic compounds with aluminium, the anodic dissolution peaks could be ascribed to the aluminium from different intermetallic compounds, having naturally different dissolution potentials. This was confirmed by the GIXRD, EMPA and AES analysis.

Alloying of copper with aluminium in the under-

Table 7. Corresponding potential values of observed plateaux in “open circuit” measurements, partial molar free energy of aluminium $\Delta\bar{G}_{\text{Al}}$ and free energy of formations ΔG_{f} of the assumed phases calculated at two temperatures

t (°C)	200			300		
	Phase composition	Inflection point (V vs. Al)	$\Delta\bar{G}_{\text{Al}}$ (kJ mol ⁻¹)	ΔG_{f} (kJ mol ⁻¹)	Inflection point (V vs. Al)	$\Delta\bar{G}_{\text{Al}}$ (kJ mol ⁻¹)
$\delta + \varepsilon_2$	0.16	-46.3	-55.6	0.22	-62.4	-34.7
$\gamma_1 + \delta$	0.3	-86.8	-61.1	0.28	-81	-34.2
$\alpha_2 + \gamma_1$	0.49	-141.8	-65.2	–	–	–
$\alpha_2 + \text{s. s. of Al in Cu}$	0.69	-199.7	-51.9	0.63	-182.4	-32.6
E_{rev} (V vs. Al)	0.9	-260.5		0.78	-225.8	

potential region becomes more pronounced with increasing melt temperature, indicating that diffusion of aluminium in the solid state becomes faster at higher temperatures.

4.4. Calculation of Gibbs energy of formation from potentiostatic data

The potential-time graphs obtained during low-current galvanostatic stripping (“open circuit” measurements) probably provide the most accurate estimates of the reversible aluminium potential corresponding to the phases on the copper surface, as well as for the reversible potential of copper (E_{rev} V vs. Al). This is because the low current gave rise to the negligible activation overpotential; the measured potential showed no immediate change when the current was interrupted.

Applying the Nernst equation [60] to the potentials reported in Table 3 gives information on the partial molar Gibbs energy of aluminium existing on the surface of copper at various times. This is constant when pairs of phases co-exist at the substrate surface, except for E_{rev} V vs. Al, where flattening of the top end of the curve, Fig. 3, merely reflects the fact that aluminium becomes exhausted at the surface after some time. To arrive at the Gibbs energy ΔG_{f} of a particular phase, it is necessary to perform a Gibbs-Duhem integration [61]. Following the procedure in [34, 35, 62] one should construct a graph of the partial molar Gibbs energy of aluminium as a function of aluminium/copper mole ratio, and then integrate it up to the composition of interest.

The problem is that whereas one knows the potentials and thus the values of the partial Gibbs energy of aluminium, $\Delta\bar{G}_{\text{Al}}$, corresponding to pairs of phases; one does not know ab initio which phases or concentrations of aluminium these correspond to. This information can be surmised by matching the potential plateaux to regions of the phase diagram where two phases co-exist. This procedure assumes that the phase diagram is obeyed. GIXRD and microanalysis data, which indicate which phases are actually present, can help in this matching.

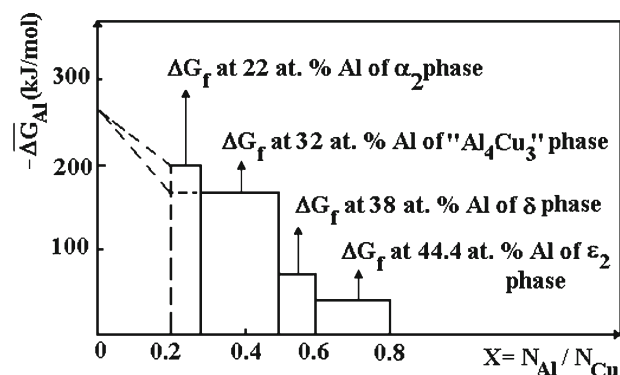


Fig. 8. Graphical representation of the calculation of (integral) free energies of formation ΔG_{f} from partial molar free energies calculated from “open circuit” plateau potentials. Data from Al in Cu at 200°C and 300°C.

Starting from Cu-rich side of the Cu-Al phase diagram [58, 59], there are seven two-phase regions at 300°C (composition limits are taken from the text of [58, 59]:

- solid solution of Al in Cu + α_2 (18.5 to 22 at.% Al);
- $\alpha_2 + \gamma_1$ or Al_4Cu_9 (23.5 to 32 at.% Al);
- $\gamma_1 + \delta$ (35.3 to 38.1 at.% Al);
- $\delta + \varepsilon_2$ (39.3 to 44.3 at.% Al);
- $\varepsilon_2 + \eta_2$ or AlCu (44.6 to 48.7 at.% Al);
- $\eta_2 + \theta$ or Al_2Cu (0.2 to 67.5 at.% Al);
- $\theta + \text{solid solution of Cu in Al}$ (67.5 to 99 at.% Al).

It is obvious from Tables 3 and 4 that the number of plateaux observed in Fig. 3, as well as the number of phases identified by GIXRD method, is less than the number of two-phase regions shown in Cu-Al phase diagram. At 200°C no plateaux are missing, so these data are used to assign phase pairs, Fig. 8. Then, at 300°C, it was assumed that the plateaux present correspond to the ones at 200°C, which occurred at very similar potentials.

The calculated values of ΔG_{f} of assumed phases are given in Table 7 together with partial molar Gibbs energy of aluminium, $\Delta\bar{G}_{\text{Al}}$, and corresponding po-

tential values of observed plateaux in “open circuit” measurements at 200 °C and 300 °C. In each case ΔG_f refers to the first phase of the quoted phase-pair (the one richer in aluminium) at its minimum-aluminium composition. No literature values for these data could be found for comparison: high temperature data cannot be extrapolated readily because of changes in the phase diagram.

As can be seen from Table 7 for data at 300 °C, the plateau corresponding to γ_1 phase in equilibrium with α_2 phase is missing. Since GIXRD data (Table 4) confirmed the presence of γ_1 , or Al_4Cu_9 , phase one can draw $\Delta \tilde{G}_{\text{Al}}$ versus concentration curve (Fig. 8) ignoring α_2 .

The Cu samples after two hours of aluminium underpotential deposition at 200 °C and 250 °C show the same unidentified GIXRD peaks. These peaks could not be ascribed to any existing Al-Cu intermetallic although the Cu sample treated at 200 °C after AES analysis showed metallic aluminium and metallic copper mixed up to a depth of 0.3 μm . In the same time AES analysis did not show presence of any impurities. This suggests that the unidentified peaks on these copper samples really arise from a new, unreported, aluminium-copper phase. According to the data available to us Al_2Cu_3 alloy has 2θ values (24.743°; 37.759°; 41.825°; 69.159°; 82.902°) closest to the unidentified peaks [64]. However, we thought these were insufficient for positive identification of our finding as Al_2Cu_3 alloy.

A possible source of error is the assumed behaviour of $\Delta \tilde{G}_{\text{Al}}$, as the mole fraction of aluminium approaches zero. The dashed line on Fig. 8 was drawn to the $\Delta \tilde{G}_{\text{Al}}$ axis, as implied by the measured open-circuit potential of copper in the electrolyte, even though in the theory the value of $\Delta \tilde{G}_{\text{Al}}$ should asymptotically approach infinity at the axis.

4.5. The growth of layers of intermetallic compounds

Figure 6 shows the thickness of the intermetallic layers, measured by Auger electron spectroscopy, and Table 6 reports the depths of the aluminium penetration obtained by EMPA and AES.

Under the assumption that the penetration depth (Δx) of the alloy into bulk substrate metal can be estimated from the equation [35, 42, 43, and 63]:

$$\Delta x = \frac{M Q_a}{z F \rho}, \quad (1)$$

where $M = 26.98 \text{ g mol}^{-1}$ and $\rho = 2.38 \text{ g cm}^{-3}$ are the atomic mass and the density of aluminium, respectively, $z = 3$ is the charge involved per atom and Q_a is the charge involved in formation of alloy after deposition at E_d vs. Al for the time τ_d . Here Q_a is taken

Table 8. Calculated slopes ($\text{mC s}^{-1/2}$) for the curves in Fig. 7

System	Temperature (°C)		
	200	250	300
Al/Cu	1.40	4.7	9.9

Table 9. The “equivalent depth” of pure aluminium (μm) into copper electrode at different temperatures

System	Temperature (°C)		
	200	250	300
Al/Cu	0.1	0.4	0.9

as the charge in excess of the value obtained from the extrapolation to τ_d , i.e. $Q_a = Q_{\text{Al},(\text{max})} - Q_{\text{Al},(\text{max})}$, $a_d = 0$. In fact this is thickness of an equivalent layer of pure aluminium, but it is difficult to make an easy correction for the density.

According to the theory expounded in [33–35], the thickness of each intermetallic layer, including buried ones, should increase with the square root of time under solid-state diffusion control. The proportionality constant depends on the difference in aluminium activity at the two-phase boundaries, as well as the mobility of aluminium.

Figure 8 shows plots of $Q_{\text{Al},(\text{max})}$ as a function of $\tau^{1/2}$ at various temperatures. Linear relationships are observed with intercepts at $\tau_d = 0$. Corresponding slopes ($\text{mC s}^{-1/2}$) for the functions in Fig. 8 are given in Table 8 for different temperatures. “Equivalent depths” of pure aluminium calculated according to Eq. (1) are given in Table 9 and are in good accord with AES and EMPA measurements (Table 6).

5. Conclusion

a) Electrochemical techniques used showed underpotential deposition of aluminium from equimolar $\text{AlCl}_3 + \text{NaCl}$ melt on copper substrate at temperatures ranging from 200 °C to 300 °C.

b) The UPD results in intermetallic compounds formation by solid state diffusion of Al into the Cu substrate. Four layers of successive intermetallic compounds could be distinguished: – solid solution of Al in Cu + α_2 (18.5 to 22 at.% Al); $\alpha_2 + \gamma_1$ or Al_4Cu_9 (23.5 to 32 at.% Al); $\gamma_1 + \delta$ (35.3 to 38.1 at.% Al); $\delta + \varepsilon_2$ (39.3 to 44.3 at.% Al). The results were consistent with established phase diagrams.

c) The diffraction patterns of copper samples, after two hours of aluminium deposition at 200 °C and 250 °C, show the diffraction peaks, which we could not attribute to any Al/Cu intermetallic compound in the data available to us. The 2θ values (degrees) for unattributable diffraction peaks are reported.

d) Linear dependence of the intermetallic layer thickness and the “characteristic aluminium penetration depth” on the square root of deposition time was confirmed by “open circuit” anodic stripping.

e) Thermodynamics shows that the constant potential regions measured during “open circuit” measurements correspond to the coexistence of pairs of intermetallic phases at the surface of copper.

f) The electrochemical potential of aluminium in a particular composition of the intermetallic compound can only be converted directly to a free energy of formation, using the Nernst equation, if neither compounds nor solution with lower concentration of Al can be formed. In general, a Gibbs-Duhem integration must be performed to arrive at free energies of formation from measured electrode potentials.

References

- [1] BRENNER, A.: Electrodeposition of Alloys. New York, Academic Press 1963.
- [2] GORBUNOVA, K. M.—POLUKAROV, Y. M.: In: Advances in Electrochemistry and Electrochemical Engineering. Ed.: Tobias, C. W. New York, Wiley 1967.
- [3] DESPIĆ, A. R.—JOVIĆ, V. D.: In: Modern Aspects of Electrochemistry. Ed.: White, R. E. New York, Plenum Press 1995.
- [4] BUDEVSKI, E.—STAIKOV, G.—LORENZ, W. J.: Electrochemical Phase Formation and Growth. Weinheim, VCH 1996. [doi:10.1002/9783527614936](https://doi.org/10.1002/9783527614936)
- [5] SMITH, W. F.: Structures and Properties of Engineering Alloys. New York, McGraw Hill Book Company 1981.
- [6] SCORDILIS-KELLEY, C.—FUULLER, J.—CARLIN, R. T.: J. Electrochem. Soc., 139, 1992, p. 694. [doi:10.1149/1.2069286](https://doi.org/10.1149/1.2069286)
- [7] STAFFORD, G. R.—JOVIĆ, V. D.—HUSSEY, C. L.: Materials Science Forum, 352, 2000, p. 49. [doi:10.4028/www.scientific.net/MSF.352.49](https://doi.org/10.4028/www.scientific.net/MSF.352.49)
- [8] TSUDA, T.—HUSSEY, C. L.—STAFFORD, G. R.: J. Electrochem. Soc., 152, 2005, p. C620.
- [9] CHEN, P.-Yu.—HUSSEY, C. L.: Electrochim. Acta, 52, 2007, p. 1857. [doi:10.1016/j.electacta.2006.07.049](https://doi.org/10.1016/j.electacta.2006.07.049)
- [10] AUSTIN, L. W.—VUCICH, M. G.—SMITH, E. J.: J. Electrochem. Tech., 1, 1963, p. 267.
- [11] DELIMARSKII, Y. K.—MAKOGON, V. F.—KUZMOVICH, V. V.: Zashch. Metal., 4, 1968, p. 743.
- [12] STAFFORD, G. R.—HUSSEY, C. L.: In: Advances in Electrochemical Science and Engineering. Vol. 7. Eds.: Alkire, R. C., Kolb, D. M. Wiley-VCH Verlag GmbH 2001.
- [13] MAMANTOV, G.—HUSSEY, C. L.—MARASSI, R.: In: Techniques for Characterization of Electrodes and Electrochemical Processes. Eds.: Varma, R., Selman, J. R. New York, John Wiley and Sons 1991, p. 471.
- [14] JOVIĆ, V. D.—JOVIĆEVIĆ, J. N.: J. Appl. Electrochemistry, 19, 1989, p. 275.
- [15] JAFARIAN, M.—GOBAL, F.—DANAEE, I.—MAHJANI, M. G.: Electrochim. Acta, 52, 2007, p. 5437. [doi:10.1016/j.electacta.2007.02.068](https://doi.org/10.1016/j.electacta.2007.02.068)
- [16] STAFFORD, G. R.—HAARBERG, G. M.: Plasmas and Ions, 1, 1999, p. 35. [doi:10.1016/S1288-3255\(99\)80010-0](https://doi.org/10.1016/S1288-3255(99)80010-0)
- [17] UEDA, M.—KIGAWA, H.—OHTSUDA, T.: Electrochim. Acta, 52, 2007, p. 2515. [doi:10.1016/j.electacta.2006.09.001](https://doi.org/10.1016/j.electacta.2006.09.001)
- [18] TIERNEY, B. J.—PITNER, W. R.—MITCHELL, J. A.—HUSSEY, C. L.—STAFFORD, G. R.: J. Electrochem. Soc., 145, 1998, p. 3110. [doi:10.1149/1.1838772](https://doi.org/10.1149/1.1838772)
- [19] CARLIN, R. T.—WILKES, J. S.: In: Chemistry of Nonaqueous Solutions. Eds.: Mamantov, G., Popov A. I. New York, VCH Publishers 1994, p. 277.
- [20] ABBOT, A. P.—McKENZIE, K. J.: Phys. Chem. Chem. Phys., 8, 2006, p. 4265.
- [21] GEETHA, S.—TRIVEDI, D. C.: Bulletin of Electrochemistry, 19, 2003, p. 37.
- [22] HUSSEY, C. L.: In: Electroanalytical Chemistry in Molten Salts. Eds.: Kissinger, P. T., Heinmann, W. R. New York, Marcel Dekker 1996, p. 511.
- [23] KOLB, D. M.: In: Advances in Electrochemistry and Electrochemical Engineering. Eds.: Gerischer, H., Tobias, C. W. New York, Wiley 1978, p. 125.
- [24] KOLB, D. M.: In: Advances in Electrochemical Science and Engineering. Vol. 7. Eds.: Alkire, R. C., Kolb, D. M. Weinheim, Wiley-VCH 2001.
- [25] BEWICK, A.—JOVIĆEVIĆ, J. N.—THOMAS, B.: Faraday Symposia of the Chem. Soc., 12, 1977, p. 24.
- [26] JOVIĆ, V. D.—JOVIĆEVIĆ, J. N.—DESPIĆ, A. R.: In: Zbornik referatov 8. Jugoslovenski Simpozij o Elektrokemiji, Dubrovnik. Ed.: Dolar, D. Ljubljana, Katedra za Fizikalno kemijo, Univerze E. Kardelja v Ljubljani 1983, p. 151.
- [27] JOVIĆEVIĆ, J. N.—JOVIĆ, V. D.—DESPIĆ, A. R.: Electrochim. Acta, 29, 1984, p. 1625.
- [28] JOVIĆ, V. D.—JOVIĆEVIĆ, J. N.: Electrochim. Acta, 30, 1985, p. 1455.
- [29] JOVIĆEVIĆ, J. N.—BEWICK, A.: Facta Universitatis, Series Physics, Chemistry and Technology, 3/2, 2005, p. 183.
- [30] THAMBIDURAI, C.—KIM, Y.-G.—STICKNEY, J. L.: Electrochim. Acta, 53, 2008, p. 6157. [doi:10.1016/j.electacta.2008.01.003](https://doi.org/10.1016/j.electacta.2008.01.003)
- [31] HUANG, J. F.—SUN, I. W.: J. Electrochem. Soc., 149, 2002, p. E348.
- [32] HSIU, S. I.—TAI, C. C.—SUN, I. W.: Electrochim. Acta, 51, 2006, p. 2607. [doi:10.1016/j.electacta.2005.07.042](https://doi.org/10.1016/j.electacta.2005.07.042)
- [33] RADOVIĆ, B. S.: The growth and characterization of novel Al surface coatings prepared by underpotential deposition from low temperature melts. [PhD thesis]. Glasgow, University of Strathclyde 1992.
- [34] RADOVIĆ, B. S.—EDWARDS, R. A. H.—JOVIĆEVIĆ, J. N.: J. Electroanal. Chem., 428, 1997, p. 113.
- [35] RADOVIĆ, B. S.—EDWARDS, R. A. H.—CVETKOVIĆ, V. S.—JOVIĆEVIĆ, J. N.: Kovove Mater., 48, 2010, p. 55. [doi:10.4149/km.2010.1.55](https://doi.org/10.4149/km.2010.1.55)

- [36] JOVIĆ, V. D.: J. Serb. Chem. Soc., 71, 2006, p. 373. [doi:10.2298/JSC0604373J](https://doi.org/10.2298/JSC0604373J)
- [37] JOHNSTON, M.—LEE, J. J.—CHOTTINER, G. S.—MILLER, B.—TSUDA, T.—HUSSEY, C. L.—SCHERSON, D. A.: J. Phys. Chem. B, 109, 2005, p. 11296. [doi:10.1021/jp051243m](https://doi.org/10.1021/jp051243m), PMID:16852379
- [38] STAFFORD, G. R.—KONGSTEIN, O. E.—HAARBERG, G. M.: J. Electrochem. Soc., 153, 2006, p. C207.
- [39] BORT, H.—JUTTNER, K.—LORENZ, W.—STAIKOV, G.: Electrochim. Acta, 28, 1983, p. 993. [doi:10.1016/0013-4686\(83\)85177-9](https://doi.org/10.1016/0013-4686(83)85177-9)
- [40] BONDOS, J. C.—GEWIRTH, A. A.—NUZZO, R. G.: J. Phys. Chem., 100, 1996, p. 8617. [doi:10.1021/jp960569f](https://doi.org/10.1021/jp960569f)
- [41] VIDU, R.—HARA, S.: J. Electroanal. Chem., 475, 1999, p. 171. [doi:10.1016/S0022-0728\(99\)00354-X](https://doi.org/10.1016/S0022-0728(99)00354-X)
- [42] VIDU, R.—HARA, S.: Surface Sci., 452, 2000, p. 229. [doi:10.1016/S0039-6028\(00\)00327-7](https://doi.org/10.1016/S0039-6028(00)00327-7)
- [43] VIDU, R.—HIRAI, N.—HARA, S.: Phys. Chem. Chem. Phys., 3, 2001, p. 3320. [doi:10.1039/b010250o](https://doi.org/10.1039/b010250o)
- [44] GARCIA, S. G.—SALINAS, D. R.—STAIKOV, G.: Surface Sci., 57, 2005, p. 9. [doi:10.1016/j.susc.2004.11.037](https://doi.org/10.1016/j.susc.2004.11.037)
- [45] ZELL, C. A.—ENDRES, F.—FREYLAND, W.: Phys. Chem. Chem. Phys., 1, 1999, p. 697.
- [46] MORIMITSU, M.—TANAKA, N.—MATSUNAGA, M.: Molten Salts XIII, 19, 2002, p. 671.
- [47] ZHU, Q.—HUSSEY, C. L.—STAFFORD, G. R.: J. Electrochem. Soc., 148, 2001, p. C88.
- [48] YAN, Y. D.—ZHANG, M. L.—HUE, Y.—HAN, W.—CAO, D. X.—HE, L. Y.: J. Appl. Electrochemistry, 39, 2009, p. 455. [doi:10.1007/s10800-008-9693-1](https://doi.org/10.1007/s10800-008-9693-1)
- [49] ABBOT, A. P.—EARDLEY, C. A.—FARLEY, N. R.—GRIFFITH, G. A.—PRATT, A.: J. Appl. Electrochemistry, 31, 2001, p. 1345. [doi:10.1023/A:1013800721923](https://doi.org/10.1023/A:1013800721923)
- [50] ZELL, C. A.—FREYLAND, W.: Chemical Physics Letters, 337, 2001, p. 293. [doi:10.1016/S0009-2614\(01\)00214-7](https://doi.org/10.1016/S0009-2614(01)00214-7)
- [51] LEE, J. J.—BAE, I. T.—SCHERSON, D. A.—MILLER, B.—WHEELER, K. A.: J. Electrochem. Soc., 147, 2000, p. 562. [doi:10.1149/1.1393233](https://doi.org/10.1149/1.1393233)
- [52] KIM, J. Y.—KIM, Y. G.—STICKNEY, J. L.: Journal of Electroanalytical Chemistry, 621, 2008, p. 205. [doi:10.1016/j.jelechem.2007.10.005](https://doi.org/10.1016/j.jelechem.2007.10.005)
- [53] GREELEY, J.—NORSKOV, J. K.: Electrochim. Acta, 52, 2007, p. 5829. [doi:10.1016/j.electacta.2007.02.082](https://doi.org/10.1016/j.electacta.2007.02.082)
- [54] JOVIĆEVIĆ, J. N.: A study of the initial stages of the electrochemical deposition of lead and thallium on copper. [Ph.D. Thesis]. Southampton, Southampton University 1978.
- [55] Joint Committee on Powder Diffraction Standards, Powder Diffraction File 4-0838.
- [56] Joint Committee on Powder Diffraction Standards, Powder Diffraction File 4-0787.
- [57] Joint Committee on Powder Diffraction Standards, Powder Diffraction File 2-1254.
- [58] MURRAY, J. L.: International Metals Reviews, 30, 1985, p. 211.
- [59] McALISTER, A. J.: Bull. Alloy Phase Diagrams, 8, 1987, p. 6. [doi:10.1007/BF02879428](https://doi.org/10.1007/BF02879428)
- [60] NERNST, W.: Z. Phys. Chem., 4, 1889, p. 129.
- [61] KUBASCHEWSKI, O.—EVANS, E. L.: Metallurgical Thermochemistry. New York, Pergamon 1958.
- [62] DARKEN, L. S.—GURRY, R. W.: Physical Chemistry of Metals. New York, McGraw-Hill 1953.
- [63] SALVAREZZA, R. C.—VASQUEZMOLL, D. V.—GIORDANO, M. C.—ARVIA, A. J.: J. Electroanal. Chem., 213, 1986, p. 301. [doi:10.1016/0022-0728\(86\)80210-8](https://doi.org/10.1016/0022-0728(86)80210-8)
- [64] DURLU, N.—GRUBER, U.—PIETZKA, M.—SCHMIDT, H.: J. Z. Metallkd., 88, 1997, p. 390.